Supplementary Material to *Cold-swappable DNA gels*
F. Bomboi, D. Caprara, J. Fernandez-Castanon and F. Sciortino

### A. DNA sequences: Swapping system

We report here the sequences designed to self-assemble the nano-star and the dimer.

$A$ particle sequences:
5'- GCGTGACTAGGGCGAAGTACCAGCGAGCGTGCAAACGCTCCACGGAGTCCGCAGTCCAGTGTAACC - 3'
5'- CGTGCTCGCACAGTGACATCTGACGACGCTGGTACTTCGCCCTAGTCACGCCAGTCCAGTGTAACC - 3'
5'- CGCTGACCCGTGGGAATCAGTTCGCACGTCAGATGTCACTGTGCGAGCACGCAGTCCAGTGTAACC - 3'
5'- CGGACTCCGTGGAGCGTTTGCACGCAGCGAACTGATTCCCACGGGTCAGCGCAGTCCAGTGTAACC - 3'

$B$ particle sequences:
5'- CGGTCACATGTCCCGGACCTCTGCGGGTTACACTGG - 3'
5'- CGCAGAGGTCCGGGACATGTGACCGACACTGGACTG - 3'.

### B. DNA sequences: Non-Swapping (no toehold) system

To demonstrate the different dynamics exhibited by *swapping* and *non-swapping* samples we modify the $A$ and $B$ particle sequences eliminating the toehold. Therefore, we keep unchanged the four arms of $A$ particles and vary only the $P$ sticky sequence, now composed of 11 instead of 15 non-self complementary basepairs. $B$ particles are composed by the same linear segment of 25 basepairs terminating on both ends with the $E2$ $ACACTGGACTG$ sequence. When $P$ and $E2$ are bonded, no free single-stranded regions are left to act as toehold. Thus, the presence of free $B$ links in solution can not start the strand exchange process. The new sequences for the $A$ and $B$ nano-structures are reported below.

$A$ particle sequences:
5'- GCGTGACTAGGGCGAAGTACCAGCGAGCGTGCAAACGCTCCACGGAGTCCGCAGTCCAGTGT - 3'
5'- CGTGCTCGCACAGTGACATCTGACGACGCTGGTACTTCGCCCTAGTCACGCCAGTCCAGTGT - 3'
5'- CGCTGACCCGTGGGAATCAGTTCGCACGTCAGATGTCACTGTGCGAGCACGCAGTCCAGTGT - 3'
5'- CGGACTCCGTGGAGCGTTTGCACGCAGCGAACTGATTCCCACGGGTCAGCGCAGTCCAGTGT - 3'

$B$ particle sequences:
5'- CGGTCACATGTCCCGGACCTCTGCGACACTGG ACTG- 3'
5'- CGCAGAGGTCCGGGACATGTGACCGACACTGGACTG - 3'.

### C. Melting profiles: NUPACK analysis

To confirm the thermodynamic binding behaviour of the selected sequences we use the NUPACK [1] oligo simulator. Based on the Santalucia thermodynamics model [2], NUPACK allows for a precise calculation of the melting temperature for the $A$ and $B$ particles as well as for the $P-E1$ and $P-E2$ complexes. By inserting the proper strands and salt concentration (fixed at the experimental value of 0.4 $M$ of NaCl for all sequences), the program calculates the $T$-dependence of the fraction of unbounded basepairs. Fig. S1 shows the calculated melting profiles. The difference between the melting $T$ of the particles and the melting $T$ of the sticky sequences confirms that the formation of the $A$ and $B$ particles takes place at significantly higher $T$ than the binding of the $P-E1$ and $P-E2$ sticky sequences. This difference in $T$ guarantees a net separation between the self-assembly of the nano-structures and the formation of the network.

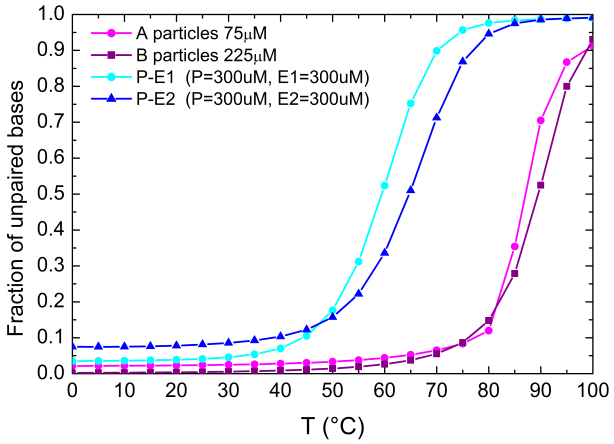


Figure S1: Melting curves calculated by using NUPACK [1]. Note that the self-assembly of the $A$ and $B$ particles precedes on cooling the binding of the sticky sequences ($P$ with $E1$ and $P$ with $E2$). Around 50 °C all possible bonds are formed.

### D. Binary mixtures of tetravalent and bivalent particles: Stockmayer theory.

The Flory and Stockmayer polymerisation theory focuses on the calculation of the gel point and of the cluster size distribution of branched structures of functionality $f$ [3]. Neglecting the formation of cycling structures and assuming equally reactive sites, the theory provides an explicit expression for the percolation point and for the cluster size distribution. We review here the theory for the case of a binary mixture of tetravalent $A$ ($f_A = 4$) and bivalent $B$ ($f_B = 2$) particles where only $AB$ bonds are allowed. Defining $N_A$ and $N_B$ as the number of $A$ and $B$ particles respectively, the probabilities $p_A$ and $p_B$ that a randomly chosen $A$ or $B$ reactive site (the sticky sequence in the DNA particle case) is involved into a bond can be expressed as

$$p_A = \frac{N_{bonds}}{4N_A}\,, \qquad p_B = \frac{N_{bonds}}{2N_B}\,, \tag{1}$$

where $N_{bonds}$ is the overall number of formed bonds. Since $A$ can only bind with $B$, $N_{bonds}$ connects $p_A$ with $p_B$. Eliminating $N_{bonds}$ from one of the two relations one finds

$$p_A = p_B \frac{N_B}{2N_A}\,. \tag{2}$$

A perfect network in which all sites are bonded is obtained at low $T$ only when $N_B = 2N_A$. At such stoichiometric composition $x \equiv N_A/(N_A + N_B)$, Eq. 2 shows that $p_A = p_B = 1$. Varying the composition from the perfect network value $x = 0.\bar{3}$, some of the reactive sites of the majority species will not be able to participate in a bond, despite the low $T$. In particular, when $x < 0.\bar{3}$ the maximum number of bonds remain equal to $4N_A$ since all $A$ sites are involved in a bond (and hence $p_A = 1$) but a finite fraction of $B$ sites remains unbounded ($p_B < 1$). The opposite case takes place for $x > 0.\bar{3}$.

The cluster size distribution $N(n, l)$, where $n$ and $l$ stand for the number of $A$ and $B$ particles in a cluster of size $n + l$ respectively, derived by Stockmayer [3] has the following expression (with $n - 1 \leq l \leq 1 + 3n$)

$$N(n,l) = f_A N_A \frac{(1-p_A)(1-p_B)}{p_B} \frac{(f_A n - n)!(2l - l)!}{(f_A n - n - l + 1)!(l - n + 1)! n! l!} x_f^n x_2^l\,, \tag{3}$$

where

$$x_{f_A} = p_B \frac{(1-p_A)^{f_A - 1}}{(1-p_B)}\,, \qquad x_2 = p_A \frac{(1-p_B)}{(1-p_A)}\,. \tag{4}$$

The condition $n - 1 \leq l \leq 1 + 3n$ arises from the fact that a cluster with $n$ tetramers must contain at least $n - 1$ and at most $1 + 3n$ links. In the particular case when $p_A = 1$, all $A$ reactive sites must be connected to a $B$ particle and hence the value of $l$ is fixed to $l = 3n + 1$.

The percolation threshold as derived by Stockmayer [3] fulfills

$$p_A p_B = \frac{1}{f_A - 1}\,. \tag{5}$$

When $p_A = 1$, the value of $p_B$ is fixed by the stoichiometry of the mixture (see Eq. 2) to $p_b = \frac{2x}{1-x}$.
The percolation threshold for $f_A = 4$ is thus given by

$$\frac{2x}{1-x} = \frac{1}{3}\,, \qquad \text{or} \qquad x = \frac{1}{7}\,.$$

Fig. S2 shows the fraction of particles in the infinite cluster as a function of $x$ as predicted by Stockmayer [3]. It is zero for $x < \frac{1}{7}$, approaches one at the stoichiometric value $x = \frac{1}{3}$ and then goes to zero again in the opposite limit in which $A$ particles are the majority component at $x = \frac{3}{5}$.

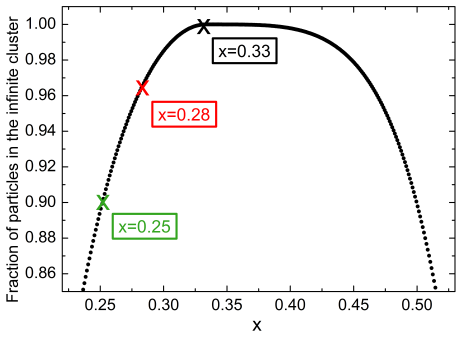


Figure S2: Fraction of particles in the infinite cluster as a function of the system composition $x$. The specific $x$ values used in the experiment are highlighted.

We experimentally select three different compositions, $x = 0.33$, $x = 0.28$ and $x = 0.25$, in which the 100%, the 96% and the 90% respectively of particles belong to the infinite spanning cluster (see crosses in Fig. S2). All the selected $x$ values are thus well beyond the percolation threshold. To provide a feeling of the three different studied concentrations we report in Table S1 the compositions $x$, the corresponding $p_B$, the fraction of unreacted $B$ sites $2(1 - p_B)$ and the fraction of $B$ particles in monomeric form $(1 - p_B)^2$.

For completeness, we show in Fig. S3 the Stockmayer's predictions for the cluster size distribution at low $T$ ($p_A = 1$) on changing $x$.

| x | $p_B$ | fraction of unreacted $B$ sites | fraction of unreacted $B$ particles |
|---|---|---|---|
| 0.33 | 1 | 0 | 0 |
| 0.28 | $0.\bar{7}$ | 0.44 | 0.05 |
| 0.25 | $0.\bar{6}$ | 0.67 | 0.11 |

Table S1: The table reports the three experimental compositions with the relative probability $p_B$ that a $B$ site is involved in a bond at low $T$ ($p_A = 1$), the fraction of unreacted $B$ sites and the fraction of unreacted $B$ particles.

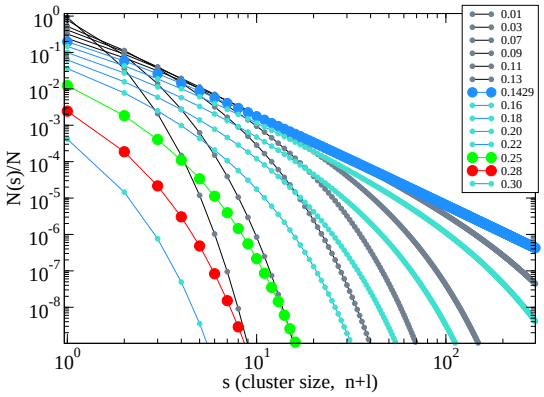


Figure S3: Normalized cluster size distribution when $p_A = 1$ (low $T$) for different values of $x$. $s$ is the sum of bi-functional ($l$) and tetra-functional ($n$) particles composing the cluster. Gray lines indicate $x$ values smaller than the percolation threshold ($x = 1/7$). Light cyan indicates $x$ values larger than the percolation threshold ($x = 1/7$). The three curves with larger symbols indicate respectively percolation (where a power-law is observed) and the distributions for $x = 0.25$ (green) and $x = 0.28$ (red).

### Theoretical Stokmayer predictions - $A$ particles with generic functionality

The same formulas, previously presented for the case $f_A = 4$, can be also expressed in a general form for particles with functionality $f_A$, always keeping the $B$-particle functionality fixed to two. The previous Eq. 1 becomes

$$p_A = \frac{N_{bonds}}{f_A N_A}\,, \qquad p_B = \frac{N_{bonds}}{2N_B}\,, \tag{6}$$

and correspondingly

$$p_A f_A N_A = p_B 2N_B\,. \tag{7}$$

The stoichiometric composition $x_{fb}$ (i.e. $p_A = p_B = 1$) is now

$$\frac{f_A x_{fb}}{2(1 - x_{fb})} = 1\,. \tag{8}$$

giving $x_{fb} = \frac{2}{5}$ for $f_A = 3$, $x_{fb} = \frac{1}{3}$ for $f_A = 4$ and $x_{fb} = \frac{2}{7}$ for $f_A = 5$. The corresponding percolation $x$ values are, from Eq. 5, $x = 0.25$ for $f_A = 3$, $x = 0.14$ for $f_A = 4$ and $x = 0.09$ for $f_A = 5$ for the $x < x_{fb}$ and $x = 0.57$ for $f_A = 3$, $x = 0.60$ for $f_A = 4$ and $x = 0.62$ for $f_A = 5$ for the $x > x_{fb}$. Fig. S4 shows the fraction of particles belonging to the infinite cluster as a function of $x$, as predicted by Stockmayer [3], for $f_A = 3, 4, 5$. On increasing $f_A$, the range of $x$ values, where a gel phase is present, increases.

## E. Phase diagram for different particle functionalities

Changing $f_A$ has also an effect on the phase diagram of the system. On a general ground, on decreasing $f_A$, the region of thermodynamic stability in the density-density or density-composition plane increases. On decreasing $f_A$ homogeneous networks can be produced with smaller average densities, resulting in floppier structures. The stability fields, for binary mixtures of limited-valence particles with functionality $f_A$ and two, can be calculated as discussed in Ref. [4] and are here reproduced in Fig. S5. The same figure reports also the associated (mean-field) percolation lines. As can be seen, the increase of $f_A$ implies a decrease of the percolation threshold, meaning that the system more easily forms a percolating spanning network. At the same time, working at high $f_A$ values results in a widening of the coexisting region. This widening reflects the increase of the density of the optimal (stoichiometric) network, a phenomenon typical of limited valence particles [5]. The experimentally investigated value $f_A = 4$ has been selected

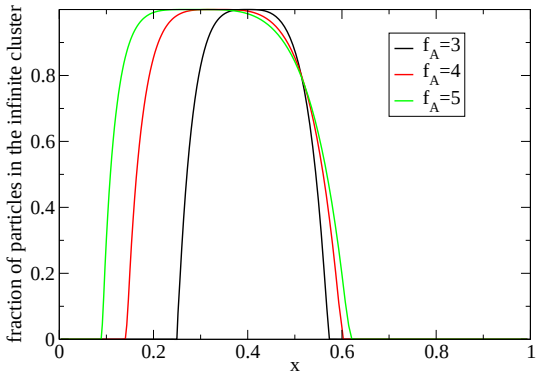


Figure S4: Fraction of particles in the infinite cluster in function of the system composition $x$ for three different values of $f_A$.

as a compromise between thermodynamic stability which decreases on increasing $f_A$ and percolation ability which increases on increasing $f_A$. It should also be noted that the increase of the network density associated to the increase of $f_A$ also brings to variations of the elastic properties of the material, as recently demonstrated for DNA nano-stars of different valence [6].

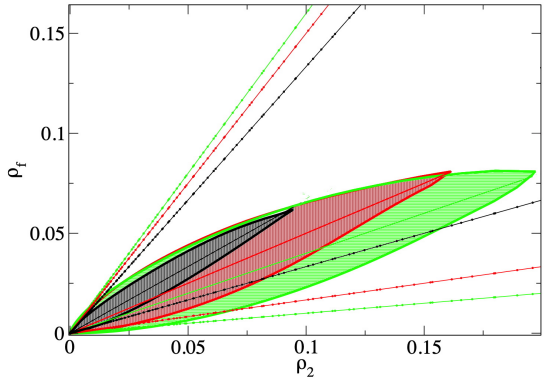


Figure S5: Phase diagram of a generic binary mixture of limited-valence particles for three different values of $f_A$ in the dimer number density $\rho_2$ and the $f$ functional particles number density $\rho_{f_A}$ plane (black $f_A = 3$, red $f_A = 4$ and green $f_A = 5$) in the fully-bonded limit. Dashed regions indicate phase-coexistence. The coexistence lines have been calculated as in Ref. [4] (Courtesy of E. Locatelli). The symbol-decorated lines indicate the mean-field percolation thresholds. Between the two symbol-decorated lines there is a space spanning cluster. The full lines inside the shaded areas indicate the stoichiometric ratios.

### F. Bulk Viscosity

DLS microrheology lies within the class of passive microrheology techniques, which consists on tracking the motion of colloidal tracers with predefined radius $\sigma$, but without directly induce any external force on them. In this scenario, it becomes possible to extract the corresponding bulk viscosity of the medium in which the tracers undergo a pure Brownian diffusion process.

In particular, we evaluate the time $t_{1/e}$ at which $g_1(t_{1/e}) = 1/e$, with $e \equiv 2.7182$, which for a pure diffusive process is equivalent to $(Dq^2)^{-1}$. Fig. S6 shows the autocorrelation functions of polystyrene (PS) colloids of radius $\sigma = 530$ nm, coated with polyethylene oxide (PEO), diffusing in the system of composition $x = 0.25$.

The selected volume fraction of colloids $\phi = 3.7 \cdot 10^{-4}$ is large enough to guarantee that the scattering is essentially

originating from the colloidal tracer particles, but low enough to preserve conditions of no inter-traces interactions. The single decay, reported for the autocorrelation functions, confirms the appropriateness of the chosen experimental conditions. The value of $\eta$ is calculated via the Stokes-Einstein relation

$$\eta = \frac{k_B T q^2}{6\pi\sigma} t_{1/e}\,, \tag{9}$$

where $k_B$ is the Boltzmann constant.

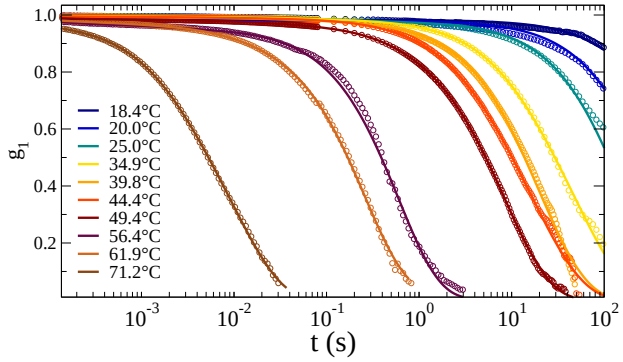


Figure S6: Measured autocorrelation functions (circles) for a system with $x = 0.25$ in the presence of a volume fraction of tracer colloids $\phi = 3.7 \cdot 10^{-4}$. The diffusive motion of the traces provides a measure of the system bulk viscosity via the Stokes-Einstein relation.

### G. Decay of the density fluctuation in a denser swapping (with toehold) system

We characterise here the $T$-behaviour of a system at $x = 0.25$, i.e. the same composition as the samples discussed in the main article, in which we increase the total density by a factor $4/3$ (e.g. the $A$ particle concentration is here fixed to 100 $\mu$M, instead of the 75 $\mu$M value reported in the main text). The concentration of B particles satisfies $x = 0.25$. Fig. S7(a-b) shows $g_1(t)$ for different $T$ for the two densities and the corresponding $\tau_s$ (in panel c). Despite the experimental noise, $\tau_s$ of the denser sample is faster, suggesting that the closer proximity of the defect tip to the toehold favours the swapping process [7].

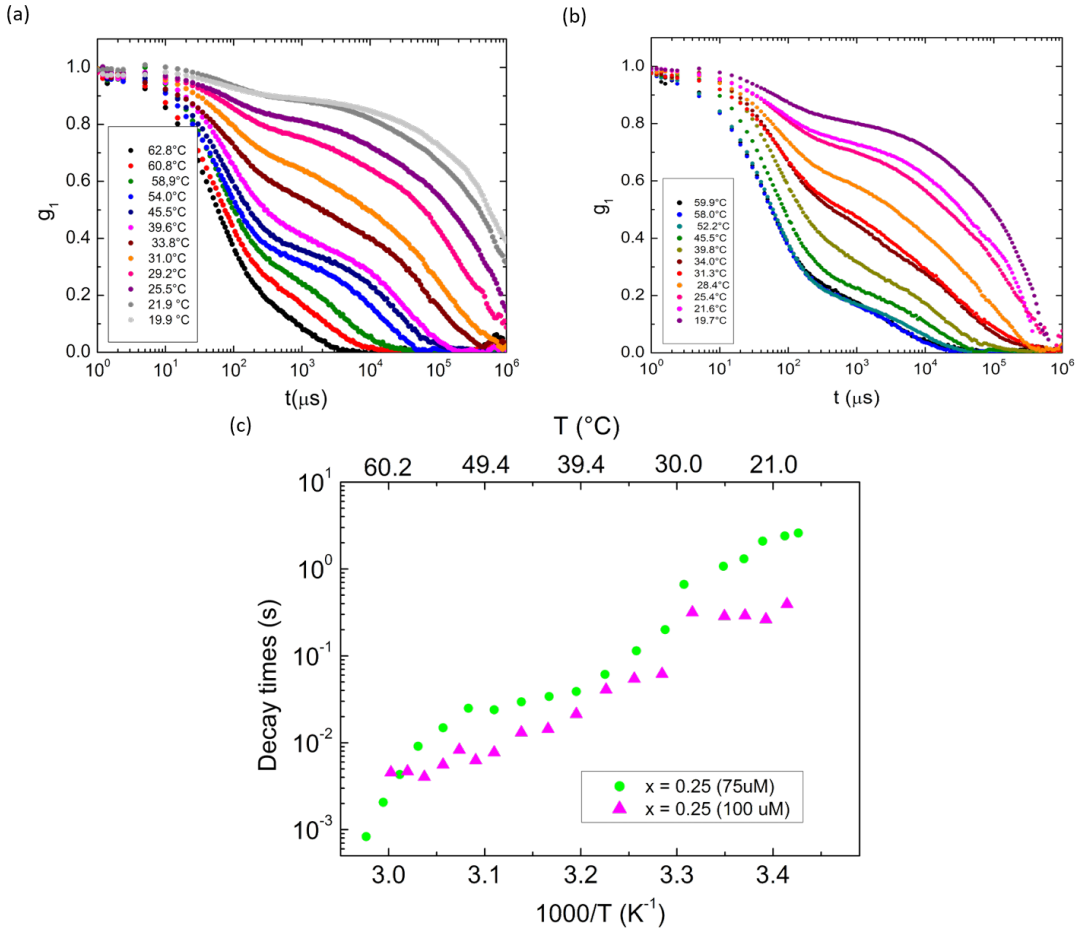


Figure S7: Correlation functions of two different samples at $x = 0.25$ differing from the $A$ particle concentrations: 75 $\mu M$ (a) and 100 $\mu M$ (b). (c) Decay times $\tau_s$ of the two systems.

### H. Acknowledgment

We thank Emanuele Locatelli for providing us with the coexistence curves shown in Fig. S5.

[1] J. N. Zadeh, C. D. Steenberg, J. S. Bois, B. R. Wolfe, M. B. Pierce, A. R. Khan, R. M. Dirks and N. A. Pierce, *J. Comput. Chem.*, 2011, **32**, 170–173.
[2] J. SantaLucia Jr and D. Hicks, *Annu. Rev. Biophys. Biomol. Struct.*, 2004, **33**, 415–440.
[3] W. H. Stockmayer, *J. Chem. Phys*, 1943, **11**, 45–55.
[4] F. Smallenburg, L. Leibler and F. Sciortino, *Phys. Rev. Lett.*, 2013, **111**, 188002.
[5] E. Bianchi, J. Largo, P. Tartaglia, E. Zaccarelli and F. Sciortino, *Phys. Rev. Lett.*, 2006, **97**, 168301–168304.
[6] Salah, *Proc. Natl. Acad. Sci. U.S.A.*, 2019, **in press**, xxx.
[7] N. Park, S. H. Um, H. Funabashi, J. Xu and D. Luo, *Nat. Mater.*, 2009, **8**, 432.